Available online at www.sciencedirect.com

ScienceDirect

journal homepage: www.elsevier.com/locate/issn/15375110

Research Paper

Developing object-based image procedures for classifying and characterising different protected agriculture structures using LiDAR and orthophoto

*Arti Tiwari, Micha Silver, Arnon Karnieli**

The Remote Sensing Laboratory, Jacob Blaustein Institutes for Desert Research, Ben-Gurion University of the Negev, Beer-Sheva 85105, Israel

ARTICLE INFO

Article history:
Received 17 March 2020
Received in revised form
20 July 2020
Accepted 24 July 2020

Keywords:
Protected agriculture
Greenhouses
Net-houses
Object-based classification
LiDAR
Orthophoto

Controlled environment conditions inside protected agriculture (PA) structures can lead to the development of sustainable agriculture. In developed countries, the rapid growth of technology of sustainable, environmentally friendly agriculture via greenhouses or net-houses is due to the significant changes in climate and increasing demand for quality products such as vegetables, fruits, herbs, etc. Therefore, there is a need to map and classify different types of PAs to help understand the pattern of crop production. Using remote sensing, the mapping of PAs has gained significant consideration in recent decades. The main goal of this study is to develop a cost-effective, novel approach to create object-based image procedures for classifying and characterising different structures of PAs. To fulfil this goal, the project integrates high-resolution orthophoto and LiDAR data. Eleven distinctive major PA classes were identified, differing in size, height, construction, shape, materials and orientation. The research was conducted over a cluster of PAs, in the Arava Valley, Wadi Araba, Israel, and demonstrated an overall accuracy and Kappa index of agreement (KIA) 92% and 0.91, respectively. Remote information and discrimination of different types of structures within a PA cluster can provide important data to decision-makers, managers, environmental protection officers and others. Authorities might infer data about the number of farms, what is being cultivating and when, or, if the PA is abandoned. Such information can also be used for quantifying damage, for predicting the dispersion of virus and help strategic planning.

1. Introduction

Protected agriculture (PA) is a general term that refers to an intensive and dynamic form of crop production where crops are grown within a variety of enclosed spaces, such as greenhouses, plastic houses and net-houses in an attempt to modify the micro-climate inside the structures to achieve optimal plant growth (El Ghoumari, Tantau, & Serrano, 2005; Nordey et al., 2017). This cultivation technique has significant advantages compared to traditional open-field practices for the farmer, for nations and from a global perspective.

* *Corresponding author.*
E-mail addresses: arti@post.bgu.ac.il (A. Tiwari), silverm@post.bgu.ac.il (M. Silver), karnieli@bgu.ac.il (A. Karnieli).
https://doi.org/10.1016/j.biosystemseng.2020.07.017
1537-5110/

Nomenclature

PA	Protected Agriculture
LiDAR	Light Detection and Ranging
KIA	Kappa index of agreement
OBIA	Object-based Image Analysis
RGB	Red–Green–Blue
DTM	Digital Terrain Model
DSM	Digital Surface Model
nDSM	Normalised Digital Surface Model
HM	Height Model
SM	Slope Model
GPS	Global Positioning System

Intensive agriculture in PAs needs fewer running expenses in terms of water and chemicals. Furthermore, yield and quality can be substantially increased and improved in comparison with open field production (Rouphael, Kyriacou, Petropoulos, De Pascale, & Colla, 2018). Farmers may also benefit by controlling the timing of the production, thus marketing their products out of season when the prices are higher. Also, affordable and sustainable PA structures, in marginally non-productive areas, could alleviate global problems of water scarcity and food security.

PAs are intended mainly for screening and reducing excessive sunlight and controlling the micro-climate (humidity, temperature, ventilation, air composition) and reducing damages caused by radiation, hot or cold weather, wind, snow and hail (Ben-Yakir, Antignus, Offir, & Shahak, 2012). In greenhouses, CO_2 can be controlled and enriched for improved photosynthesis (Katzir, 2015). PAs are designed for saving irrigation water, fertiliser and pesticides. Net covering can protect from birds, pests and insects, as well as diseases and viruses.

There is a wide range of PAs that can be distinguished by their type, height, material, density, colour, shape and design, as well as the crops cultivated. Type is principally referred to either as a greenhouse or net-house. Three levels of PA heights are known – mulch is a non-elevated layer of synthetic material that covers the soil surface (Merle & Jensen, 1995). Floating row covers and low tunnels are usually used to cover a bed row, whilst high tunnels/shelters, up to 4 m height, cover a much larger area of a plant system. The height of the structure is also one of the significant features that directly impacts on natural ventilation, creating a natural 'chimney effect' that controls atmosphere and crop management inside the greenhouse. PA cover materials, which influence the quality of the indoor micro-climate, range from row covers and mulching systems (either organic, petroleum or plastic) to a large variety of glass and plastic polymers (Von Elsner et al., 2000b; Waaijenberg, 2006). There are also different widths and colours to modify the spectral composition of the transmitted and reflected sunlight (Ben-Yakir et al., 2012). The net covering can be in different densities (Legarrea, Karnieli, Fereres, & Weintraub, 2010).

A vast diversity of crops is grown in PAs. These range from vegetables and flowers to fruit trees such as grapevines, bananas and citrus. The crops are grown either directly on the ground, on lifted soil-less beds or hanging from above on the construction. The building materials of PAs can be either timber, bamboo, galvanised steel or aluminium. The structural designs of the roof include different shapes (e.g., pitched, round-arches, saw-tooth shed and Gothic arched roofs), orientation, and inclination that determine the total light transmittance and ventilation (Von Elsner et al., 2000a; Waaijenberg, 2006).

Originally, PAs were developed and used in developed countries (Von Elsner et al., 2000b). They enable the growing season to be extended and crop varieties expanded. However, since land and water resources have become a significant limitation for food production in large parts of the world, knowledge transfers and international interests made it possible to extend this technology to less affluent regions of the world (Merle & Jensen, 1995). As a result, PAs currently exist all over the globe, including the tropical, semi-arid/arid, temperate and polar regions, as well as in urban locations (McCartney & Lefsrud, 2018). In 2018, the global area of PA structures was estimated as ~3,400,000 ha, where 15% of this area was greenhouses (https://www.hortidaily.com/article/6040786/greenhouse-vs-protected-agriculture-vegetable-production/), and their area is gradually increasing. This increase has raised the need to map and classify different PAs and thus infer their expansion at local, regional and national scales, along with the type of crops that could be potentially grown.

Despite the large variety of PA structures, two standard features make it possible to fulfil the above goal. The first is their geometrical design, i.e., a rectangle for an individual PA and a tabular structure for a cluster of PAs. The second is their light-translucent covers that are partially transparent to solar radiation. In this regard, two remote sensing products can be used: (1) very high-resolution imaging; and (2) Light Detection and Ranging (LiDAR) data. High-resolution imagery distinguishes fine details, allowing for image classification to identify different PAs. However, performing automatic classification of features when depending only on their spectral characteristics is challenging, especially in spectrally homogeneous regions. Object-based image analysis (OBIA) methods approach this problem by integrating both spectral and spatial characteristics of objects (Myint, Gober, Brazel, Grossman-Clarke, & Weng, 2011) and LiDAR takes advantage of the transparency of PA covers. LiDAR records the laser pulses and their reflected intensity, separately, from the upper top of the object (the PA roof) and the surface (soil and vegetation). LiDAR therefore offers high-precision 3D spatial point cloud information and is widely applied in various applications and directions (Flood, 2001). Also, LiDAR is an essential tool for producing elevation models and thereby deriving slopes.

Most of the reviewed studies have been focused only on the mapping one type of PA structure, e.g., plastic greenhouse, glass greenhouse or net-house. Several high-resolution satellite images were compared by Carvajal, Agüera, Aguilar, and Aguilar (2011) for detecting greenhouses in south-eastern Spain. Based on WorldView-2 images, a comparison of various classification methods for glass and plastic greenhouses identification and differentiation was performed by Koc-San (2013). Tarantino and Aiello (2011) applied an object-based classification method to classify the plastic-covered

vineyards from aerial true-colour data. Greenhouse differentiation using the maximum likelihood classification method, was carried out by Agüera & Liu, 2009 using the separation and categorisation of the similar objects merged with calibration and a pseudo-calibration processes with QuickBird and IKONOS images.

Several studies reported, an object-based method with LiDAR in many applications, such as land cover classification, the mapping of structural types of forest and forest gap identification, etc (Antonarakis, Richards, & Brasington, 2008; Mao & Hou, 2019; Ruiz, Recio, Crespo-Peremarch, & Sapena, 2018). However, the authors are not aware of any study that distinguishes between different PAs using object-based classification and LiDAR data. The overarching goal of the current paper is to demonstrate a procedure to discriminate and classify various structures of PAs. Since PAs exhibit several structural features, remote sensing data at very high resolution, such as ortho-rectified aerial photography (orthophotos), together with LiDAR, can be considered an appropriate means for fulfilling the goal. Therefore, the study hypothesis asserts that structural features can be extracted by applying an object-based classification approach using a data fusion method. Airborne orthophotos and LiDAR systems provide complementary datasets that synergistically enable discriminating, classifying and mapping elevated PAs of various sizes, heights, constructions, shapes, materials and orientations.

2. Study area and data source

The research was implemented at one greenhouse cluster located in the Arava Valley, Wadi Araba, Israel, south of the Dead Sea basin and part of the Rift Valley (30° 82′N 35° 27′E) (Fig. 1). The total size of the cluster is 1405 × 2019 m (ca. 3 km^2). The size of each plot is 100 × 100 m (0.01 km^2).

The area has exceptional climatic and geographic features, raising opportunities and challenges for farmers. The climate is hyper-arid, which is characterised by very low rainfall (25–50 mm year^{-1}), high temperatures (~40 °C in the summer), low humidity and high solar radiation. These conditions are a challenge to local growers. Yet after more than 50 years of settlement in this area, and with support of the local agricultural research and development centre, profitable agriculture has been achieved by the successful application of PAs (https://www.eaci.co.il/arava-center-israel).

Eleven major classes of structure were identified in the study site (Fig. 2): *Low plastic tunnel; Net-house; Circular net-house, Porched cut edge shape; Saw-tooth structure; Arched shape; Edge arched shape; Net stretched under arched shape; Circular arched shape; Circular wide arched shape;* and *Circular arched shaped with 90° rotation*. All these structures consisted of plastic film or nets (or a combination of the two) supported by a metal construction.

Two different data sets were used, airborne LiDAR imagery and an orthophoto. LiDAR data was acquired on 27 Oct. 2012 using the ALTM 3100EA (enhanced accuracy) instrument of Optech Incorporated at a density of 2 points per m^2. Then digital elevation models were prepared from this point cloud at 1 m spatial resolution with 0.1 m vertical accuracy. The other data was a true-colour (RGB) aerial photograph with standard spectral red–green–blue bands that was obtained in 2010. This photograph, after geometric correction and orthorectification, produced an image at 0.25 m resolution and uniform scale that enabled accurate distance measurements. Only slight differences, of three ground structures, were

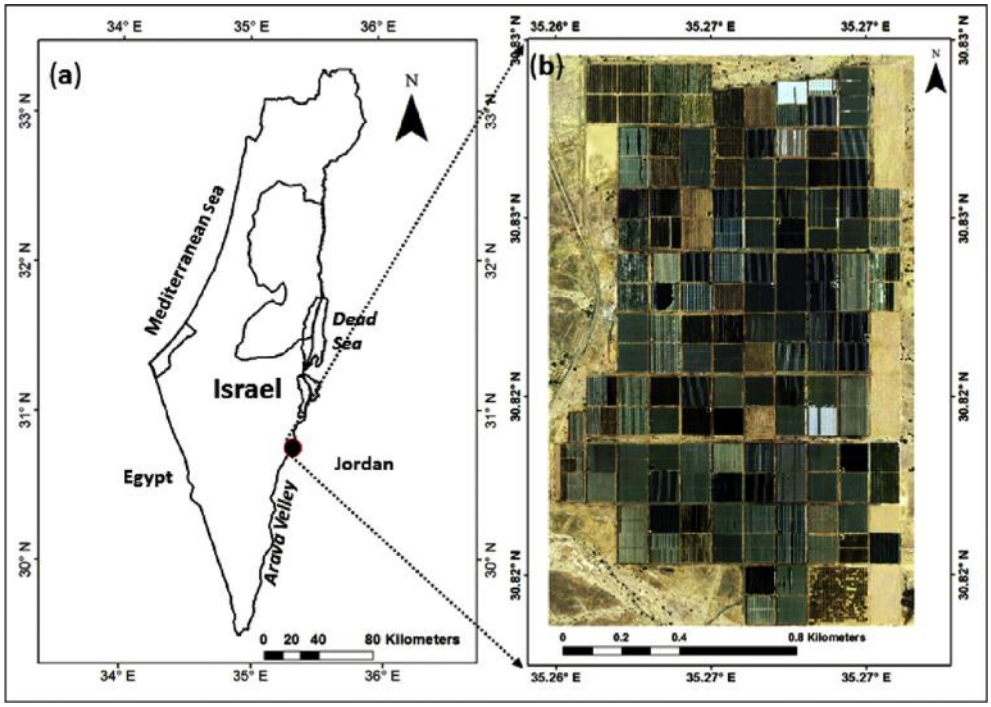

Fig. 1 – (a) Location of the study area in Israel; (b) True-colour (RGB) ortho-rectified aerial photography (orthophotos) of the study site.

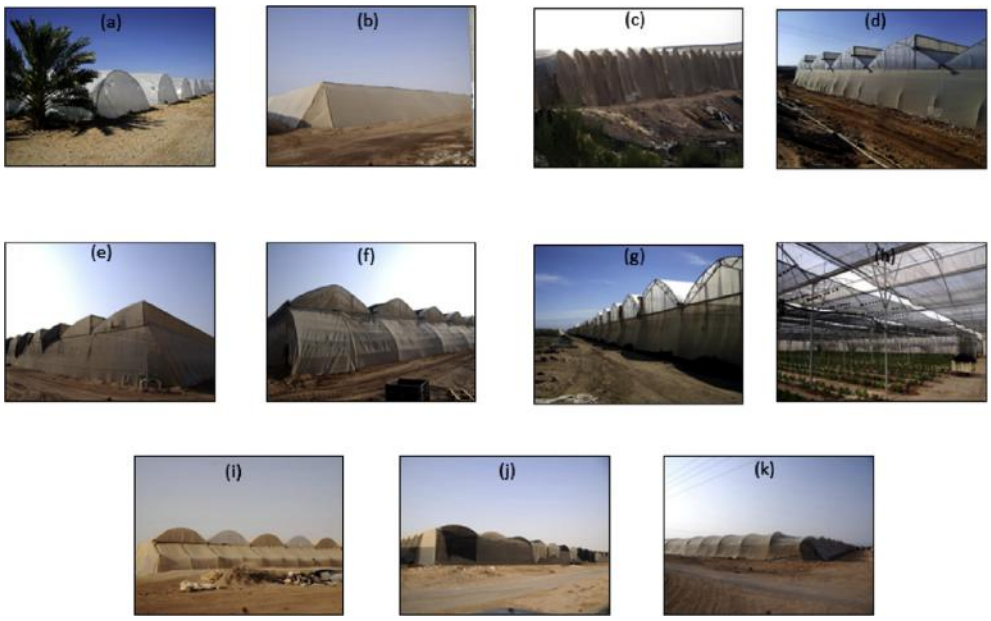

Fig. 2 – Different types of PAs structures. (a) Low plastic tunnel; (b) Net-house; (c) Circular net-house; (d) Porched cut edge shape; (e) Saw-tooth structure; (f) Arched shape; (g) Edge arched shape; (h) Net stretched under arched shape; (i) Circular arched shape; (j) Circular wide arched shape; (k) Circular arched shape with 90° rotation.

observed between LiDAR and the aerial photograph acquisition dates (see Appendix-A).

3. Methods

3.1. *LiDAR surface derivations*

The applied methodology to perform the analysis and to generate surface models using LiDAR cloud data is presented in Fig. 3. The two common LiDAR data products are the Digital Terrain Model (DTM) that represents the elevation of the ground, and the Digital Surface Model (DSM) that provides the height of the elevated structure at each point.

The DTM was created at 1-m spatial resolution by the least elevation and referred to as the 'last return' in the LiDAR data processing terms, whereas the DSM with the highest elevation in the same pixel and referred to as the 'first return'. The DSM data were smoothed by 2D Gaussian filter to remove noise and to preserve edges with a kernel size of 3 following the Zevenbergen-Thorne method for quantitative topographic analysis (Zevenbergen & Thorne, 1987). Utilising the transparent characteristics of the PAs, the DTM was subtracted from the smoothed DSM (i.e., the differences between the first and the last returns were calculated) to create a normalised Digital Surface Model (nDSM) that is the desired Height Model (HM) of the PAs. The smoothed DSM data were also used to calculate the slopes of the elevated structure, thus created the Slope Model (SM). All models were implemented by utilising the ArcGIS 10.7.1 and eCognition Developer 9.3 software packages. The three-dimensional analysis of the different PA structures using the profiles of the LiDAR-derived first and last returns was analysed by employing ERDAS IMAGINE software.

3.2. *Classification*

An object-based rule-based approach was carried out to separate different PAs using eCognition Developer. The preliminary step in the object-based method is to perform

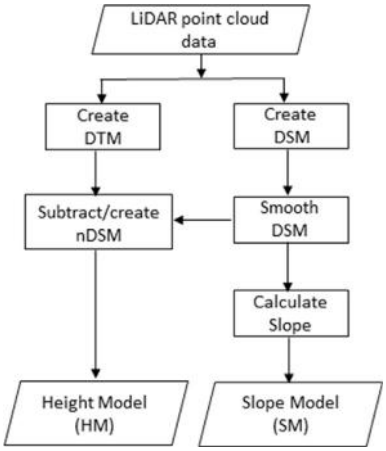

Fig. 3 – The applied methodology to generate surface models using LiDAR data: Height model (HM) and Slope model (SM).

segmentation over pixels to form objects. The segmentation procedure defines objects comprised of groups of pixels with similar feature values from the image. This technique attains user-defined homogeneity based on some attributes such as similarity in shape, size, texture, colour, etc. within each image object. The process includes merging neighbour objects that fulfil user-defined homogeneity criteria (eConition Developer, 2009).

The current study implemented a multi-level segmentation hierarchy, Level-I, Level-II and Level-III (Fig. 4). In segmentation Level-I, both orthophoto and vector map of the PAs cluster, which was generated in ArcGIS software by the on-screen digitization method, were used as an input. Applying a chessboard segmentation method, all existing PAs' clustered as an object, were extracted.

Contrast split segmentation was applied to create sub-level objects, termed hereafter as segmentation Level-II and Level-III. The algorithm further segmented an image object based on bright and dark areas depending on a threshold value. The minimum and maximum values were set to 0 and 200, respectively. This threshold maximised the difference among the nearby dark as well as bright objects. The process calculated the optimum threshold individually for each image object within the domain. If the certain pixel level was selected in the domain, the algorithm initially implements a chessboard segmentation, then carried out the split on the respective square by considering its distinctive pixel value as a potential threshold. The selection of test threshold values was according to the step size and stepping type parameter (step size of 20 and step type 'add', with contract mode 'edge-ratio' were chosen), which ranges from the minimum to maximum threshold, with intermediate values. In case the test threshold justifies the minimum dark and minimum bright area standard, the contrast between dark and bright objects was estimated. The highest contrast test threshold was selected and used for separation.

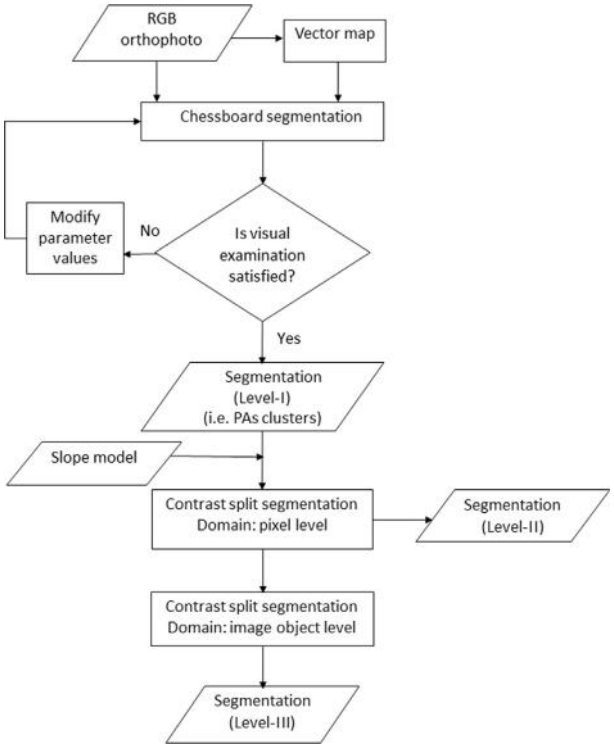

Fig. 4 – The generated image level hierarchies: segmentation Level-I, Level-II and Level-III.

All discriminated objects were segmented in Level-II, yet variations in slope were not isolated at this point. Subsequently, another segmentation step, Level-III was added to separate those, again utilising the 'contrast split segmentation', with different parameter values (minimum and maximum values were set to 80 and 200, respectively). To perform segmentation, in derived surfaces (i.e., HM and SM), the SM was used since the model expected to provide the best value data for deciding the structure of PAs. Therefore, segmentation Level-III objects was classified in classification Level-II and classification Level-III. Additional parameters for the contrast split segmentation algorithm were minimum relative dark and bright areas of 0.1, minimum contrast 0 and minimum object size 1. Accordingly, measurements were provided for each layer after segmentation that relied on pixel values within an individual object.

For classifying PA structures, object-based image classification was performed over prepared image-level hierarchies. The three-level classification (i.e., Level-I, Level-II and Level-III) was achieved. Additionally, the classification Level II scheme was comparatively crude in detail but allowed improved classification at classification Level III. Figure 5 represents the functional methodology of the initial classification. Classification Level-I contained all existing PA structures present in the study area (Fig. 5a). To extract classification, segmentation Level-I was used. Classification Level-II divided the image objects within two classes – elevated structure, and non-elevated surface (Fig. 5b). The elevated structure was identified using the HM model values. All objects with an $HM \geq 0.6$ m in the model were assigned to the elevated structure. Following, the non-elevated surface class was recognised utilising the same model. Values for $HM \leq 0.1$ m were classified as the non-elevated surface. The non-elevated surface included open areas as well as open vegetation.

This knowledge-based classification primarily followed a decision tree approach with various required rule sets and one or multi-level threshold criteria to accomplish the classification. Principally, the decision tree depended on previous knowledge (i.e., knowledge of the study area) before implementing thresholds and rules, and hence the relevance of features changed by objective. Therefore, it was essential to identify the most desirable object features for classification. The geographic location and spatial extent of the individual class were noted before performing classification. Therefore, multiple objects (i.e., group of pixels) of a recognised class were tested for their range of values from a specific surface model form, and the threshold value range was selected afterward.

The following algorithms (Eqs. 1–5) were established for Level-III classification hierarchy that separates the elevated structures into five major classes, using both HM and SM model, namely *Low plastic tunnel*; *Net-house*; *Porched cut edge shape*; *Saw-tooth structure*; and *Net stretched under arched shape*.

.		
Low plastic tunnel	$(HM < 1)$	(1)
Net-house	$(1 < HM \leq 3.6) \wedge (HM \geq 3.6 \wedge SM \leq 9.5)$	(2)
Porched cut edge shape	$(HM > 3.6) \wedge (4.3 < HM \leq 4.83 \wedge 23 < SM < 24.6) \wedge (1.43 < HM < 1.45 \wedge 44 < SM < 45) \wedge (4.9 < HM < 5 \wedge 14 < SM < 15) \wedge (1.6 < HM < 1.65 \wedge 47 < SM < 48)$	(3)
Saw-tooth structure	$(HM \geq 1.2 \wedge 37 \leq SM \leq 48.5) \wedge (HM > 4.7 \wedge 13 \leq SM \leq 20) \wedge (3.6 < HM < 4 \wedge 27 < SM < 28.6) \wedge (4.58 < HM < 4.7 \wedge 18 < SM < 20) \wedge (5.1 < HM < 5.3 \wedge 12 < SM < 13)$	(4)
Net stretched under arched shape	$(1.29 < HM < 1.36 \wedge 37.5 < SM < 41)$	(5)

Finally, Level-III classification hierarchy contained six additional classes that were merged into one single class (i.e., Other structure) (Eq. 6). The additional classes were separated based on the following algorithms (Eqs. 7–12), named *Edge arched shape*; *Arched shape*; *Circular arched shape*; *Circular wide arched shape*; *Circular arched shaped with 90° rotation and Circular net-house*.

.		
Other structure	$(3.7 < HM < 5.1 \wedge 11 < SM < 27) \wedge (5.4 < HM \leq 5.6 \wedge 14 < SM \leq 14.6) \wedge (4.7 < HM < 5.1 \wedge 14.7 < SM < 16) \wedge (5.3 < HM < 5.4 \wedge 21 < SM < 22)$	(6)
Edge arched shape	$(4.7 < HM < 5.4 \wedge 21 < SM < 27) \wedge (HM > 4.26 \wedge 26.6 < SM < 26.8)$	(7)
Circular wide arched shape	$(4 < HM < 4.6 \wedge 12 < SM < 19) \wedge (4.5 < HM < 4.6 \wedge 18 < SM < 18.4)$	(8)
Circular net-house	$(HM < 4.1 \wedge 12.5 < SM < 12.7)$	(9)
Circular arched shape with 90° rotation	$(HM > 5.5 \wedge SM > 14.5)$	(10)
Arched shape	$(4.2 < HM < 5.1 \wedge 14.5 < SM < 27)$	(11)
Circular arched shape	$(4.7 < HM < 4.8 \wedge 15 < SM < 16) \wedge (3.6 < HM < 3.8 \wedge 14 < SM < 15) \wedge (4.5 < HM < 4.6 \wedge 11 < SM < 12)$	(12)

Subsequently, damage could be identified in a particular elevated structure with the applied classification method. Finally, individual class vector layers were extracted and the total area (km^2) was calculated using ArcGIS.

3.3. Classification accuracy assessment

The classification was evaluated with ground reference information that was procured using a Garmin Global Positioning System (GPS), with 10 m accuracy, during a field campaign. A total of 419 GPS points (397-elevated structure samples, and 22-non-elevated surface) were collected in the field and compared to the classification products. The overall accuracy and Kappa coefficient were calculated from an error confusion matrix (Congalton, 1991; Foody, 2002). All the statistical calculations were performed using the eCognition software.

4. Results

4.1. LiDAR-derived surface models and profiles of PA structures

The LiDAR-derived surface models are presented in Fig. 6, including DTM (Fig. 6a), DSM (Fig. 6b), SM (Fig. 6c) and HM (Fig. 6d). The three-dimensional analysis of the PAs took advantage of the LiDAR return points. The first return was calculated from the top edges of the structures while the last return from the ground. If intermediate returns existed, they were related to a specific surface.

Figure 7 describes the profiles of the LiDAR-derived first and last returns with respect to the different PA structures (Fig. 2). Blue colour shows the first returns, extracted from the PAs edges – the top edges of the structure. The red colour exhibits the points of last returns that represented the ground.

- In the case of the *Low plastic tunnel* (Fig. 7a), two blue lines appear. One is the straight line on the bottom that means return from the ground or features exist under low plastic tunnels. The second is the upper curved line that indicates the return from the top of the structure.

In this case, the LiDAR's first and last returns of the structures could not be separated. Since the distance between the low plastic tunnel and the object/features inside is less than the LiDAR vertical resolution (i.e., 0.7 m), this PA was characterised by a single return.

- In the case of the flat roof surface, as in the *Net-house* (Fig. 7b), points are very close together in the horizontal plane and thus have similar elevations. Hence, the separation was observed between the first (net) and last (ground) returns.
- The relative thick first return in the *Circular net-house* (Fig. 7c) indicated the material and the structure of the plastic nets.
- Detecting some damage of the PA (e.g., holes or torn plastic present in the greenhouse cover) was demonstrated by the discontinuity of the first return in the *Porched cut edge shape* (Fig. 7d), where the first return is seen at the ground level or from nearby objects within the greenhouse.
- In the case of *Net stretched under arched shape* (Fig. 7h) the plastic roof was observed on top and a shading net beneath. As in the *Low plastic net*, these two could not be separated due to the short distance between them.
- The relative thickness of the first returns in the *Circular arched shape* structures (Fig. 7i–k) was due to the use of a net on top of the plastic roof. The difference between the first and the last returns indicated the height of the PA structure.
- The various structures found to be the highest, e.g., the *Porched cut edge shape*, the *Saw-tooth structure* and the *Edge arched shape*, etc. while the *Low plastic tunnel* – the lowest (Fig. 7d, e, g and a, respectively).

4.2. *Classification*

The process of classification was divided into three levels. Classification Level-I map provides a broad view of available PAs in the study area (Fig. 8a) and Level-II classification divides the image objects into two classes, elevated structures and non-elevated surfaces (Fig. 8b). Additionally, the areas with damaged structures, such as broken buildings or torn roofs, were detected and marked. A minor difference between classes was observed in the classification results (i.e., Fig. 8a and b) because of the data acquisition dates of the LiDAR (2012) and the orthophoto (2010). The difference was verified during the field visit.

The final classification (Level-III), based on Eqs. 1–12, concluded with thirteen classes, including classes of eleven elevated PAs, one class of non-elevated structure and one damaged structure (Fig. 9). The graphical representation of the total area covered by different PAs (Fig. 10) shows that most of the area was covered by three structures, i.e., *Net-house* (0.40 km^2), *Saw-tooth* covers 0.20 km^2 and 0.07 km^2 covered by *Porched cut edge shape*. Smaller areas were covered by three structures, i.e. *Circular net-house* (0.01 km^2), *Low plastic tunnel* (0.01 km^2) and *Circular arched shape with 90° rotation* (0.01 km^2). Certain structures filled the remaining area, ranging from 0.03 to 0.04 km^2.

4.3. *Accuracy assessment*

No substantial changes in the PAs had occurred between the dates of orthophoto and the LiDAR acquirement in the field campaign. However, visual inspection revealed a few minor changes. The ground reference points were matched with the final classification. The primary statistics were precise within the frame of a confusion matrix and the accuracy statistics. The final classification had an overall accuracy of 92% and a Kappa index of agreement (KIA) of 0.91 based on individual ground reference points; although a small number of structures were misclassified. Some of the errors arose from changes in the middle of collected reference ground data and the threshold values used in the rule sets to classify the SM along with HM (i.e., *Porched cut edge shape* confused with *Saw-tooth structure*) (Table 1). User accuracy (60%) and producer accuracy (80%) were low for the *Saw-tooth structure* compared to other structures (Table 1). The

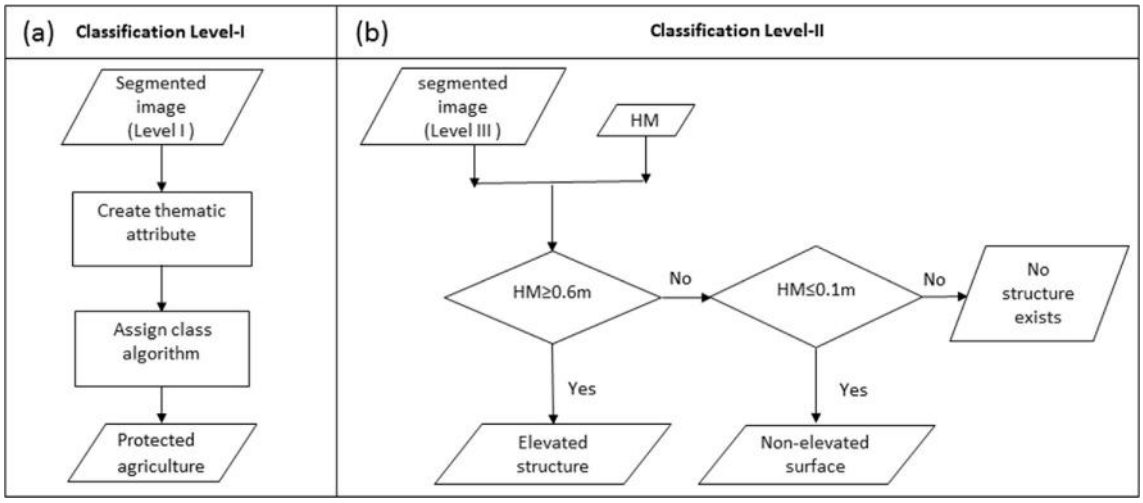

Fig. 5 – The performed methodology to achieve initial classification. (a) Classification Level I; (b) Classification Level-II.

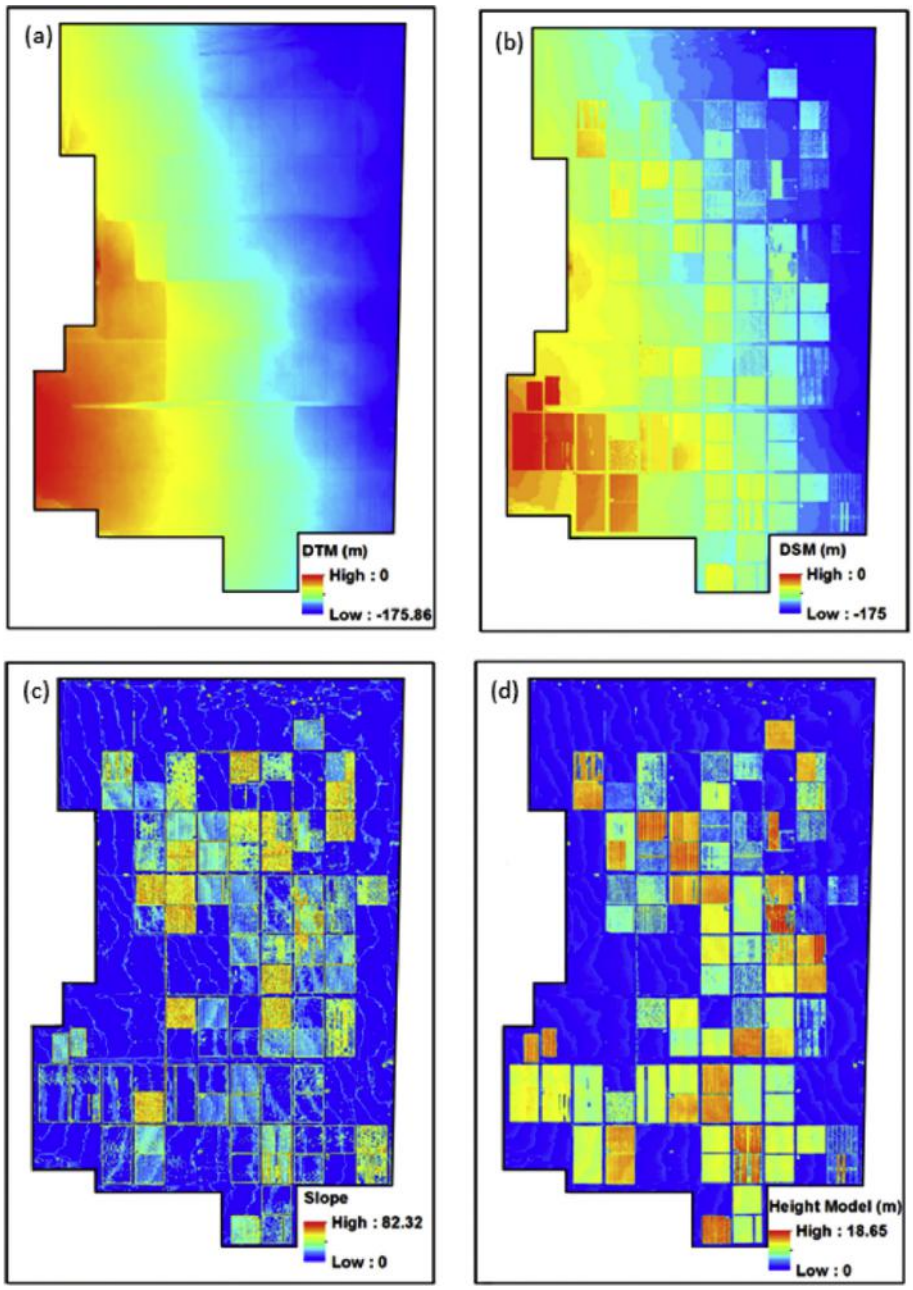

Fig. 6 – Products of the LiDAR surfaces models: (a) Digital terrain model (DTM); (b) Digital surface model (DSM); (c) Slope model (SM); (d) Height model (HM).

three classes *Low plastic tunnel, Arched shape* and *Circular net-house* had 100% user and producer accuracy, indicating that all sample object of a particular class was assigned to the same class.

5. Discussion

Each PA structure has a specific use in terms of its micro-climate, light transmittance, ventilation, etc. Incoming solar radiation, humidity, temperature, air velocity inside the PA structure and level of CO_2 are the micro-climate conditions that are essential for crop growth (Bournet & Boulard, 2010). The variables are functions of the PA structure, latitude, meteorological conditions and ventilation arrangement. The controlled conditions inside the PA structures can provide the optimal surrounding for better quality products and growth yields.

5.1. *Effectiveness of using object-based over pixel-based*

In this paper, a method was proposed to differentiate between PA structures. The pixel-based approach, which solely depends on spectral bands, is assumed to be insufficient and

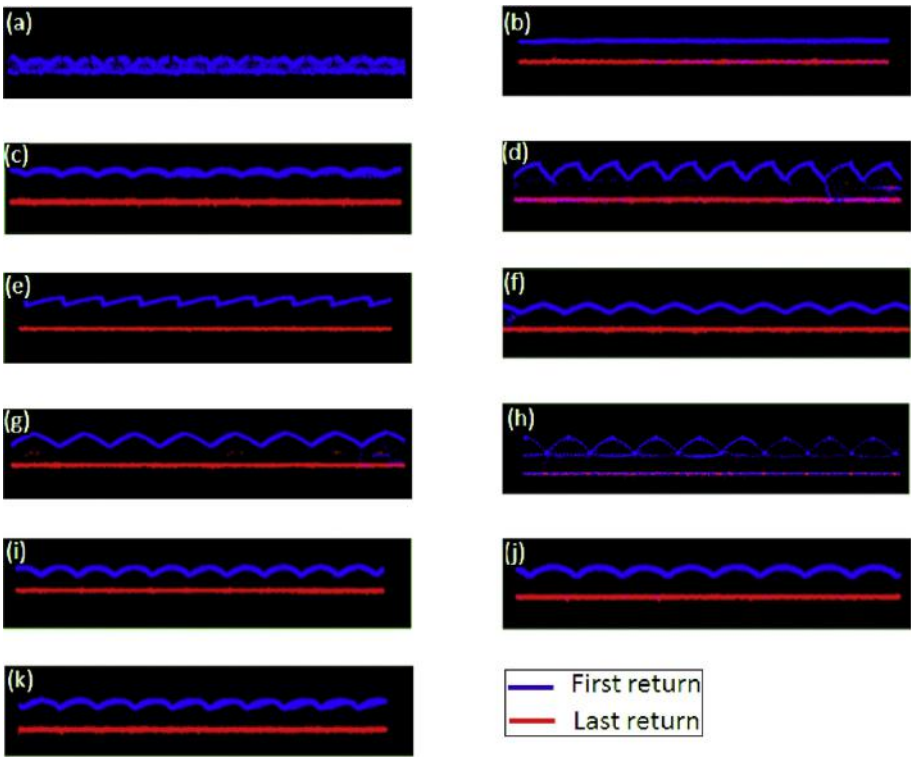

Fig. 7 – Profiles of the LiDAR-derived first and last returns along with the different PA structures (a) Low plastic tunnel; (b) Net-house; (c) Circular net-house; (d) Porched cut edge shape; (e) Saw-tooth structure; (f) Arched shape; (g) Edge arched shape; (h) Net stretched under arched shape; (i) Circular arched shape; (j) Circular wide arched shape; (k) Circular arched shape with 90° rotation.

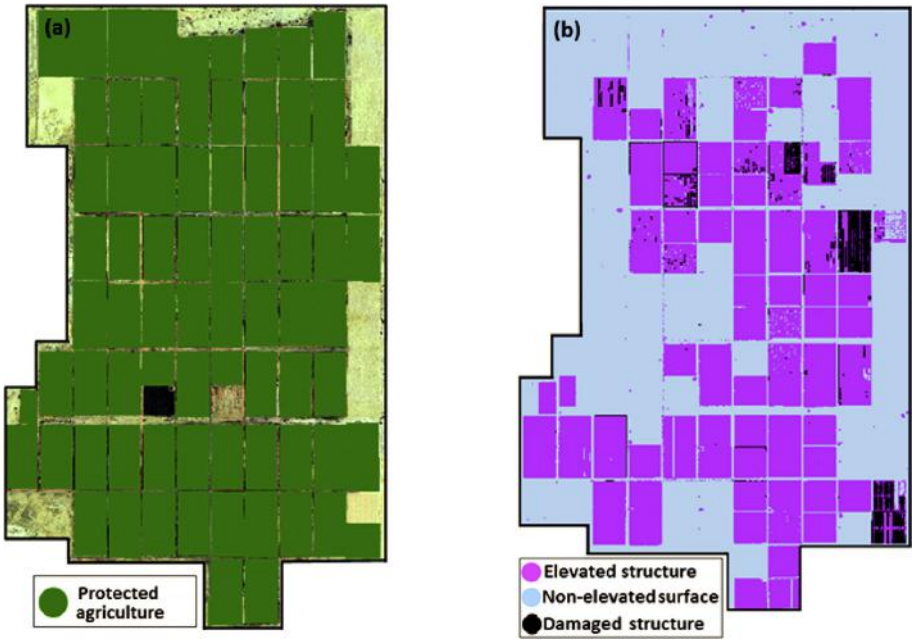

Fig. 8 – (a) Classification Level-I of all available PAs. (b) Classification Level-II of initial major classes.

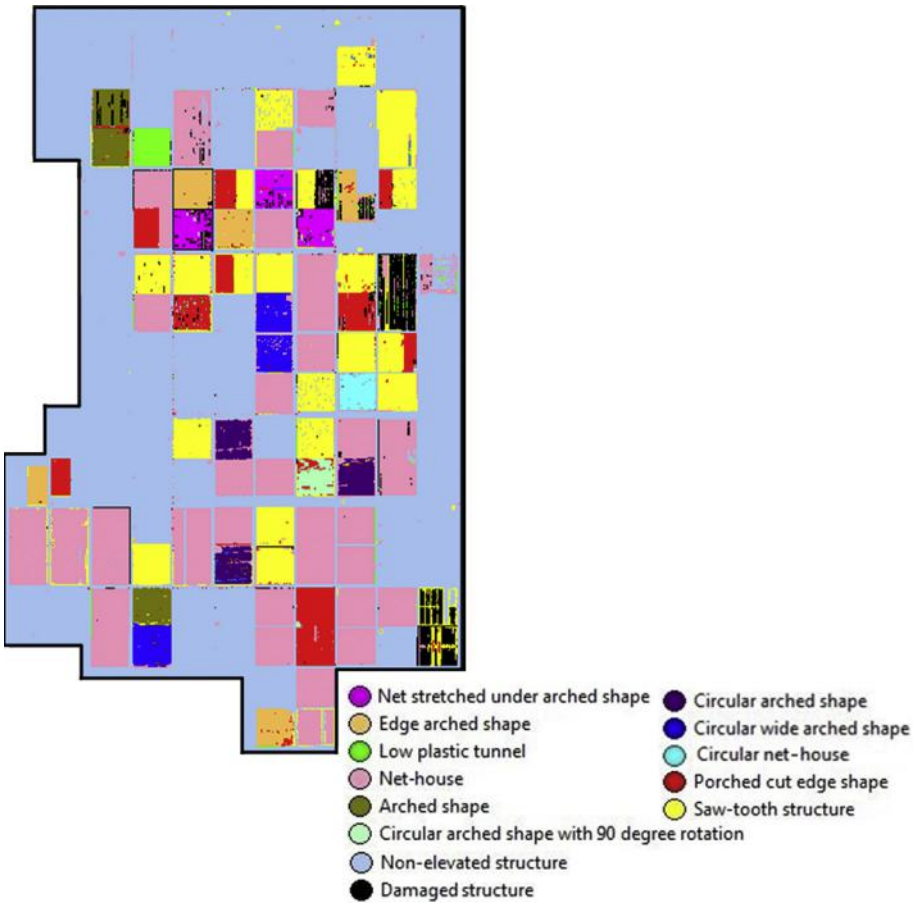

Fig. 9 – The final classification (Level-III) of elevated structure.

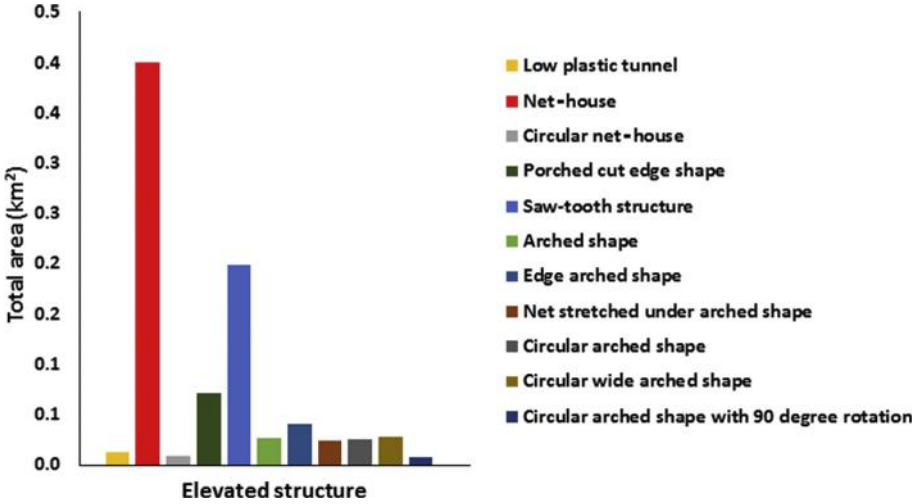

Fig. 10 – Graphical representation of total area of all type of PAs' structure in field.

Table 1 – Confusion matrix for object-based image classification (elevated structure).

Classification class	Reference class												
	Net-house	Porched cut edge shape	Low plastic tunnel	Saw-tooth structure	Net stretched under arched shape	Arched shape	Edge arched shape	Circular wide arched shape	Circular net-house	Circular arched shape	Circular arched shape with 90° rotation	Row total	User accuracy (%)
Net-house	68	0	0	0	1	0	0	5	0	1	0	75	90.7
Porched cut edge shape	2	63	0	11	0	0	0	0	0	0	4	80	78.75
Low plastic tunnel	0	0	13	0	0	0	0	0	0	0	0	13	100
Saw-tooth structure	0	8	0	12	0	0	0	0	0	0	0	20	60
Net stretched under arched shape	0	0	0	0	17	0	0	0	0	0	0	17	100
Arched shape	0	0	0	0	0	37	0	0	0	0	0	37	100
Edge arched shape	0	3	0	0	0	0	25	0	0	0	0	28	89.28
Circular wide arched shape	0	0	0	0	0	0	0	27	0	0	0	27	100
Circular net-house	0	0	0	0	0	0	0	0	17	0	0	17	100
Circular arched shape	0	0	0	0	0	0	0	0	0	37	0	37	100
Circular arched shape with 90° rotation	0	0	0	0	0	0	0	0	0	0	26	26	100
unclassified	0	0	0	0	2	0	0	0	0	1	0	3	
Column total	70	74	13	23	20	37	25	32	17	39	30		
Producer accuracy (%)	97.1	85.14	100	52.17	85	100	100	84.38	100	94.87	86.67		

Overall accuracy (%) 92%.
Kappa index of agreement (KIA) 0.91.

might result in incorrect classification. The alternative object-based image analysis (OBIA) takes advantage of both the spectral and spatial data for classification. Sets of similar pixels, termed image objects, are characterised and grouped based on their spectral information, shape, size, texture, as well as spatial contextual associations with the surrounding pixels, leading to the improved delineation of objects. The delineation of the PA structures relies on the height, slope and orientation of the detected objects. Therefore, OBIA was found to be a useful approach for extracting and classifying PAs in parallel to several recent studies that compared the two approaches (Ouyang et al., 2011; Silveira et al., 2019; Tiwari, Meir, & Karnieli, 2020; Whiteside, Boggs, & Maier, 2011).

5.2. *Advantage of LiDAR*

By using LiDAR data along with orthophoto, an object-based procedure was developed to classify and differentiate between PA structures with diverse geometrical features. The approach was successful, with the 92% overall accuracy. Eleven different types of structures were extracted and classified using the LiDAR-generated height model (HM) and slope model (SM).

LiDAR takes advantage of the transparency characteristics of the PA structure. At the same time, the laser pulses are reflected and recorded, separately, both from the upper top of the object (i.e., structure's roof) and the surface (i.e., soil and vegetation). Various feature specific algorithms for extracting information from LiDAR have been established for the different urban environments (Chen, Gong, Baldocchi, & Xie, 2007; Rottensteiner & Briese, 2002; Zhang, Yan, & Chen, 2006). Several reported studies were specifically focused on object-based procedures combined with LiDAR data, e.g., Mao and Hou (2019).

5.3. *Added values of the aerial orthophoto*

The classification results and accuracy would remain the same if only the LiDAR-derived features (i.e., slope and height) were used to classify the structures. Nevertheless, the strength of this project is by combining LiDAR and orthophoto data. In this regard, interlacement of aerial orthophoto with the LiDAR data, helps in various aspects, such as:

- Identifying the exact boundary of the all available PA cluster in the area of interest. The accurate position of the PA boundaries was calculated by the integration of the generated vector boundary map with aerial orthophoto imagery using a chessboard segmentation algorithm. Once the PA cluster region was detected, it integrates with LiDAR data to structure the roof of PAs.
- After finding the category of the PA structures, it helps to find the total area covered by the individual PA type.
- In this research, an object-based approach, using a data fusion method, was applied. There are some common standard criteria that generally used in object-based classification procedure: (a) spectral/colour information; (b) spatial information; (c) textural information; (d) size and shape information; and (e) association (i.e., relation to neighbours, relation to other objects). In these features, spectral information took from aerial orthophoto imagery that was integrated with LiDAR to classify and map structural features.

5.4. *Importance of classifying PAs*

Remote information and discrimination of different types of structures within a PA cluster can provide essential data to decision-makers, managers, environmental-protected rangers and others. Authorities might infer about the number of farmers, what they are cultivating and when, or, on the other hand, if the PA is abandoned. Water used and its efficiency can be assessed. Although most of the PAs are made of nylon, polyester net or even glass, they are usually opaque for the outside observer. However, since the type of construction fits the type of crop, it hints about which plants are grown inside. For example, low tunnels are used to grow herbs, higher structures for cucurbits or flowers and the highest for trellising tomatoes or peppers. Net-houses are used to protect banana plantations. Plastic structures are more subject to be torn. However, if the structure has a metal skeleton, it would be considered stronger and wind resistance. In this regard, since the LiDAR observations can map such damage, it can be quantified and used for insurance assessment. In terms of plant pest inspection, if diseases strike in one of the PAs, environmental protection officers can estimate the potential dispersion of the virus to other structures with a similar crop. Finally, decision-makers and planners can use remote PAs information for a future strategic plan.

6. Conclusions

In the remote sensing discipline, orthophoto and LiDAR can be analysed to obtain information related to PA structure identification. The data analysis stratagem, outlined in this work, to extract structural features resulted from applying an object-based approach using a data fusion method. This stratagem interpreted data from orthophoto, ground measured data and LiDAR to classify and map structural features in a challenging agricultural region.

The current study showed that an airborne LiDAR is a powerful tool for classifying any type of structure. The procedure was effective in precisely classifying 92% of the PA structures in the study site. Both elevation and slope information, along with orthophoto spectral images, played a part in outlining areas and achieving improved PA structure classification. After an assessment of these applied approaches, LiDAR information is self sufficient to recognise the structure, but more precise mapping obtained when combined with orthophoto. The two LiDAR-derived raster surfaces, DTM and DSM, allowed the classification into eleven different structures. LiDAR derivatives: slope and elevation data, which comprised the most pre-processing time, were essential for classification. Segmentation enabled image objects to achieve spectral, spatial and contextual features of the input layers and to properly work for LiDAR surfaces.

This data analysis approach can be utilised in numerous applications involving surveys of PA structures and alterations over time. Within the study's broader perspective, PA

structure classification data can be beneficial when correlated to the crop production rates. This information can be used to control the amount of light reaching the crop, the requirement of natural ventilation, humidity and temperature to enhance crop yield within PAs. In order to formulate future recommendations, this study might help the local ministry of agriculture to obtain an accurate picture of what crop strains are currently being grown, in which type of PA structure, and what yields are obtained. This could help to understand the actual crop pattern and their growth with a specific PA structure. Typically, baseline crop data is collected through questionnaires sent to farmers, a very time-consuming process for the collection and also in terms of data analysis. For decision-makers and managers, it might be highly desirable and/or beneficial to provide an automated system to collect baseline PA structure data and update that data periodically.

Funding

This research did not receive any specific grant from funding agencies in the public, commercial or not-for-profit sectors.

Declaration of competing interest

The authors declare that they have no known competing financial interests or personal relationships that could have appeared to influence the work reported in this paper.

Appendix-A

REFERENCES

Agüera, F., & Liu, J. G. (2009). Automatic greenhouse delineation from QuickBird and Ikonos satellite images. *Computers and Electronics in Agriculture, 66*(2), 191–200. https://doi.org/10.1016/j.compag.2009.02.001

Antonarakis, A. S., Richards, K. S., & Brasington, J. (2008). Object-based land cover classification using airborne LiDAR. *Remote Sensing of Environment, 112*(6), 2988–2998. https://doi.org/10.1016/j.rse.2008.02.004

Ben-Yakir, D., Antignus, Y., Offir, Y., & Shahak, Y. (2012). Colored shading nets impede insect invasion and decrease the incidences of insect-transmitted viral diseases in vegetable crops. *Entomologia Experimentalis et Applicata, 144*(3), 249–257. https://doi.org/10.1111/j.1570-7458.2012.01293.x

Bournet, P. E., & Boulard, T. (2010). Effect of ventilator configuration on the distributed climate of greenhouses: A review of experimental and CFD studies. *Computers and Electronics in Agriculture, 74*(2), 195–217. https://doi.org/10.1016/j.compag.2010.08.007

Carvajal, F., Agüera, F., Aguilar, F. J., & Aguilar, M. A. (2011). Relationship between atmospheric corrections and training-site strategy with respect to accuracy of greenhouse detection process from very high resolution imagery. *International Journal of Remote Sensing, 31*(11), 2977–2994. https://doi.org/10.1080/01431160902946580

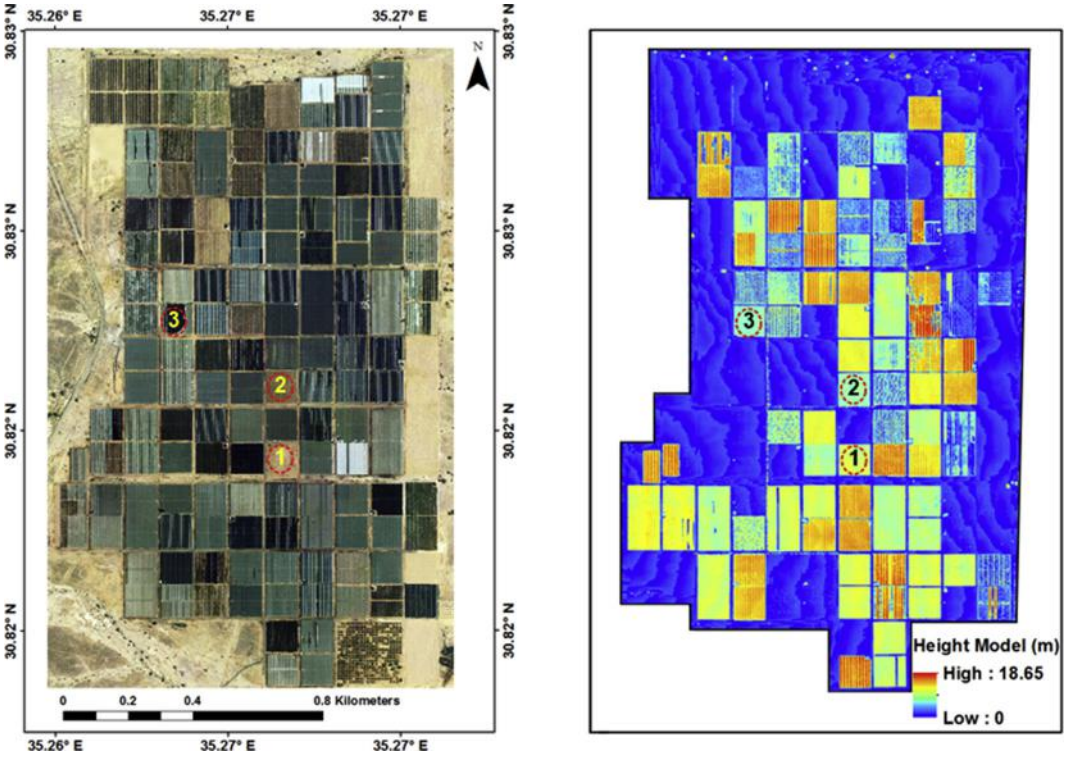

Fig. A1 – Original aerial photograph (left) vs. the HM, showing the observed differences between the orthophoto (2010) and the LiDAR (2012). Structures marked as 1 and 2, are new structures while 3 is a torn structure that was repaired.

Chen, Q., Gong, P., Baldocchi, D., & Xie, G. (2007). Filtering airborne laser scanning data with morphological methods. *Photogrammetric Engineering & Remote Sensing, 73*(2), 175–185. https://doi.org/10.14358/PERS.73.2.175

Congalton, R. G. (1991). A review of assessing the accuracy of classifications of remotely sensed data. *Remote Sensing of Environment, 37*(1), 35–46. https://doi.org/10.1016/0034-4257(91)90048-B

User Guide. (2018). *Trimble eCognition Developer 9.3*. Germany: Munich.

El Ghoumari, M. Y., Tantau, H. J., & Serrano, J. (2005). Non-linear constrained MPC: Real-time implementation of greenhouse air temperature control. *Computers and Electronics in Agriculture, 49*(3), 345–356. https://doi.org/10.1016/j.compag.2005.08.005

Flood, M. (2001). LiDAR activities and research priorities in the commercial sector. In M. A. Hofton (Ed.), *Workshop on Land Surface Mapping and Characterization using Laser Altimetry. 22-24 October 2001, Annapolis, Maryland* (Vol. 34, pp. 3–7).

Foody, G. M. (2002). Status of land cover classification accuracy assessment. *Remote Sensing of Environment, 80*(1), 185–201. https://doi.org/10.1016/S0034-4257(01)00295-4

Katzir, R. (2015). Advance agriculture in the desert: the Israeli case story. *Sciences in Cold and Arid Regions, 7*(1), 1–6. https://doi.org/10.3724/SP.J.1226.2015.00001

Koc-San, D. (2013). Evaluation of different classification techniques for the detection of glass and plastic greenhouses from WorldView-2 satellite imagery. *Journal of Applied Remote Sensing, 7*(1), Article 073553. https://doi.org/10.1117/1.jrs.7.073553

Legarrea, S., Karnieli, A., Fereres, A., & Weintraub, P. G. (2010). Comparison of UV-absorbing nets in pepper crops: Spectral properties, effects on plants and pest control. *Photochemistry and Photobiology, 86*(2), 324–330. https://doi.org/10.1111/j.1751-1097.2009.00657.x

Mao, X., & Hou, J. (2019). Object-based forest gaps classification using airborne LiDAR data. *Journal of Forestry Research, 30*(2), 617–627. https://doi.org/10.1007/s11676-018-0652-3

McCartney, L., & Lefsrud, M. (2018). Protected agriculture in extreme environments: A review of controlled environment agriculture in tropical, arid, polar, and urban locations. *Applied Engineering in Agriculture, 34*(2), 455–473. https://doi.org/10.13031/aea.1259

Merle, H., & Jensen, A. J. M. (1995). *Protected agriculture: A global review*. Retrieved from https://books.google.co.il/books?hl=en&lr=&id=F1eghGKD6bwC&oi=fnd&pg=PR7&dq=Jensen,+M.H.,+%26+Malter,+A.J.+(1995).+Protected+agriculture:+A.+In.+Washington,+D.C.&ots=upC8DqlfiE&sig=WnB_0aloT2s_FB5MgqNcA9KmlQo&redir_esc=y#v=onepage&q&f=false.

Myint, S. W., Gober, P., Brazel, A., Grossman-Clarke, S., & Weng, Q. (2011). Per-pixel vs. object-based classification of urban land cover extraction using high spatial resolution imagery. *Remote Sensing of Environment, 115*(5), 1145–1161. https://doi.org/10.1016/J.RSE.2010.12.017

Nordey, T., Basset-Mens, C., De Bon, H., Martin, T., Déletré, E., Simon, S., … Malézieux, E. (2017, December 1). Protected cultivation of vegetable crops in sub-Saharan Africa: Limits and prospects for smallholders. A review. *Agronomy for Sustainable Development, 37*. https://doi.org/10.1007/s13593-017-0460-8

Ouyang, Z. T., Zhang, M. Q., Xie, X., Shen, Q., Guo, H. Q., & Zhao, B. (2011). A comparison of pixel-based and object-oriented approaches to VHR imagery for mapping saltmarsh plants. *Ecological Informatics, 6*(2), 136–146. https://doi.org/10.1016/j.ecoinf.2011.01.002

Rottensteiner, F., & Briese, C. (2002). *A new method for building extraction in urban areas from high-resolution LiDAR data*. Retrieved from http://www.isprs.org/proceedings/xxxiv/part3/papers/paper082.pdf.

Rouphael, Y., Kyriacou, M. C., Petropoulos, S. A., De Pascale, S., & Colla, G. (2018). Improving vegetable quality in controlled environments. *Scientia Horticulturae, 234*, 275–289. https://doi.org/10.1016/j.scienta.2018.02.033

Ruiz, L.Á., Recio, J. A., Crespo-Peremarch, P., & Sapena, M. (2018). An object-based approach for mapping forest structural types based on low-density LiDAR and multispectral imagery. *Geocarto International, 33*(5), 443–457. https://doi.org/10.1080/10106049.2016.1265595

Silveira, E. M. O., Silva, S. H. G., Acerbi-Junior, F. W., Carvalho, M. C., Carvalho, L. M. T., Scolforo, J. R. S., et al. (2019). Object-based random forest modelling of aboveground forest biomass outperforms a pixel-based approach in a heterogeneous and mountain tropical environment. *International Journal of Applied Earth Observation and Geoinformation, 78*, 175–188. https://doi.org/10.1016/j.jag.2019.02.004

Tarantino, E., & Aiello, A. (2011). Plastic covered vineyard extraction from airborne sensor data with an object-oriented approach. *Remote Sensing for Agriculture, Ecosystems, and Hydrology XIII, 8174*(October 2011), 817415. https://doi.org/10.1117/12.898175

Tiwari, A., Meir, I. A., & Karnieli, A. (2020). Object-based image procedures for assessing the solar energy photovoltaic potential of heterogeneous rooftops using airborne LiDAR and orthophoto. *Remote Sensing, 12*(2), 223. https://doi.org/10.3390/rs12020223

Von Elsner, B., Briassoulis, D., Waaijenberg, D., Mistriotis, A., Von Zabeltitz, C., Gratraud, J., … Suay-Cortes, R. (2000a). Review of structural and functional characteristics of greenhouses in European Union countries: Part I, design requirements. *Journal of Agricultural and Engineering Research, 75*(1), 1–16. https://doi.org/10.1006/jaer.1999.0502

Von Elsner, B., Briassoulis, D., Waaijenberg, D., Mistriotis, A., Von Zabeltitz, C., Gratraud, J., … Suay-Cortes, R. (2000b). Review of structural and functional characteristics of greenhouses in European Union countries, part II: Typical designs. *Journal of Agricultural and Engineering Research, 75*, 111–126. https://doi.org/10.1006/jaer.1999.0512

Waaijenberg, D. (2006). Design, construction and maintenance of greenhouse structures. *Acta Horticulturae, 710*, 31–42. https://doi.org/10.17660/ActaHortic.2006.710.1

Whiteside, T. G., Boggs, G. S., & Maier, S. W. (2011). Comparing object-based and pixel-based classifications for mapping savannas. *International Journal of Applied Earth Observation and Geoinformation, 13*(6), 884–893. https://doi.org/10.1016/j.jag.2011.06.008

Zevenbergen, L. W., & Thorne, C. R. (1987). Quantitative analysis of land surface topography. *Earth Surface Processes and Landforms, 12*(1), 47–56. https://doi.org/10.1002/esp.3290120107

Zhang, K., Yan, J., & Chen, S.-C. (2006). Automatic construction of building footprints from airborne LIDAR data. *IEEE Transactions on Geoscience and Remote Sensing, 44*(9), 2523–2533. https://doi.org/10.1109/TGRS.2006.874137